Journal of Chromatography, 597 (1992) 397–410
Elsevier Science Publishers B.V., Amsterdam

CHROM. 23 814

Biospecific interaction analysis using surface plasmon resonance detection applied to kinetic, binding site and concentration analysis

Lars G. Fägerstam*, Åsa Frostell-Karlsson, Robert Karlsson, Björn Persson and Inger Rönnberg

Pharmacia Biosensor AB, S-751 82 Uppsala (Sweden)

ABSTRACT

A system for real-time biospecific interaction analysis using biosensor technology based on the optical phenomenon surface plasmon resonance is described. The biospecific interface is a sensor chip covered with a hydrogel matrix. One component of the interaction to be studied is immobilized covalently to the hydrogel and other interactants are passed over the chip in solution. The mass change at the sensor surface, reflecting the progress of the interaction studied, is monitored in real time. The technique, which does not require molecular labels for detection, can measure mass changes down to 10 pg/mm^2. Repeated analyses can be performed on the same sensor chip. Applications shown include kinetic measurements, binding site analysis and concentration determination.

INTRODUCTION

The availability of techniques for the characterization of biospecific interactions is essential for the understanding of the relationship between the structural features of molecules and their implications on interaction dynamics. Such techniques can be subdivided into two categories, "direct" and "indirect". With a direct technique the molecular interaction can be monitored without the use of labels, whereas for an indirect technique a label such as an enzyme, a fluorophore or a radioactive isotope is needed for detection. Direct optical techniques include ellipsometry [1], attenuated total internal reflection [2] and surface plasmon resonance [3].

Surface plasmon resonance (SPR) [4–6] is dependent on the resonant coupling of light, incident on a thin metal film, to oscillations of the conducting electrons, called plasmons, at the metal film surface. These oscillations give rise to an evanescent field which extends from the surface into the sample solution. When resonance occurs, the reflected light intensity drops at a sharply defined angle of incidence, the SPR angle, which is dependent on the refractive index within the reach of the evanescent field in the proximity of the metal surface. Devices for SPR sensing have been described using either the Kretschmann configuration [4] where light is internally reflected at the base of a metal film-coated prism or using metal film-coated diffraction gratings [7]. A noteworthy difference between the two approaches is that in the latter instance the sample solution has to be transparent to allow illumination of the grating. In experimental approaches described for SPR sensing [3,7–12], the specificity of detection has been obtained through adsorption of a protein (usually an antibody or antigen) to the naked metal film followed by exposure of the biospecific surface to a bulk solution of the analyte. No attempts have been made to regenerate the sensor surface, but to eliminate the need for cleaning and coating the prism between successive experiments detachable metal-coated glass slides have been used [10].

This paper describes a system for biospecific

0021-9673/92/$05.00

interaction analysis in which SPR detection is combined with a dextran-modified sensor chip to which one of the components of the interaction under study can be covalently attached. Flow-injection liquid handling allows the sequential injection of several interactants and regeneration solutions, facilitating the repeated use of the same sensor surface.

EXPERIMENTAL

Equipment and reagents

The BIAcore system, sensor chip CM5, surfactant P20 and amine coupling kit containing N-hydroxysuccinimide (NHS), N-ethyl-N′-(3-diethylaminopropyl)carbodiimide (EDC) and ethanolamine hydrochloride were obtained from Pharmacia Biosensor (Uppsala, Sweden). Insulin-like growth factors I and II (IGF I and IGF II), structural variants of IGF I, IGF binding protein 1 (IGFBP-1), anti-IGFBP-1 mouse monoclonal antibodies and IGFBP-1 derived peptides were a gift from Dr. M. Hartmanis (Kabigen, Stockholm, Sweden). *Lac* operator DNA, a synthetic 35-base pair DNA with one strand biotinylated at the 5′-end (biotin-5′-TGT GTG GAA TTG TGA GCG GAT AAC AAT TTC ACA CA-3′), was a gift from Dr. L. Holmberg (Pharmacia Biosystems, Uppsala, Sweden). Streptavidin was obtained from Sigma (St. Louis, MO, USA) and a fusion between *lac* repressor and *β*-galactosidase was obtained from Promega (Madison, WI, USA). β_2-Microglobulin and corresponding mono- and polyclonal antibodies were obtained from Pharmacia Biosystems.

Preparation of sensor surfaces

Immobilizations of proteins to the sensor chip via primary amine groups were performed in the instrument in he following manner. Separate vials containing 200 μl of 0.1 *M* NHS, 0.4 *M* EDC, 1 *M* ethanolamine hydrochloride (adjusted to pH 8.5 with sodium hydroxide) and 100 m*M* HCl and a vial for mixing EDC and NHS were placed in the autosampler together with a solution of protein in the appropriate buffer. The continuous-flow pump was filled with HBS [10 m*M* 4-(2-hydroxyethyl)-1-piperazineethanesulphonic acid (HEPES), 0.15 *M* NaCl, 3.4 m*M* EDTA, 0.05% surfactant P20 adjusted to pH 7.4 with sodium hydroxide]. After conditioning of the sensor chip with HBS, the automated immobilization cycle was performed at a flow-rate of 5 μl min^{-1}; 70 μl each of EDC and NHS were transferred to the mixing vial, after which 30 μl were injected to activate the carboxymethylated dextran matrix. The protein solutions were then injected followed by 35 μl of ethanolamine to deactivate any remaining activated carboxyl groups. Individual conditions for all immobilized substances are given in Table I.

All other experimental details are given in the figure captions.

Surface plasmon resonance detection principle

Surface plasmon resonance is an optical phenomenon arising in connection with total internal reflection of light at a metal film–liquid interface. Normally, light travelling through an optically denser medium, *e.g.*, a glass prism, is totally reflected back into the prism when reaching an interface to an optically less dense medium, *e.g.*, a buffer, provided

TABLE I

IMMOBILIZATION CONDITIONS

Ligand	Concentration (μg ml^{-1})	Volume (μl)	Buffer (pH)	Activation time (s)	Amount immobilized (RU)	Regeneration
IGF-I	50	10/25	4.75	420	630/1325	100 m*M* HCl
IGF-II	50	25	4.75	420	1600	100 m*M* HCl
IGFBP-1	50	25	4.75	420	3340	100 m*M* HCl
RAMFc	100	30	4.75	420	7000–9900	100 m*M* HCl
Streptavidin	200	35	4.5	420	5000	–
Anti-$\beta_2\mu$ MAb	30	30	5.0	240	13 000	10 m*M* HCl/pH 2.2

that the angle of incidence is larger than the critical angle. This is known as total internal reflection. Although the light is totally reflected, a component of the incident light momentum called the evanescent wave penetrates a distance of the order of one wavelength into the buffer. The evanescent wave may be used to excite molecules close to the interface, as in total internal reflection fluorescence [13]. If, however, the light is monochromatic and *p*-polarized and the interface between the media is coated with a thin (a fraction of the light wavelength) metal film, the evanescent wave under certain conditions will interact with free oscillating electrons (plasmons) in the metal film surface. When surface plasmon resonance occurs, light energy is lost to the metal film and the reflected light intensity is thus decreased. The resonance phenomenon will only occur for light incident at a sharply defined angle which, when all else is kept constant, is dependent on the refractive index in the buffer close to the surface. Changes in the refractive index out to about 1 μm from the metal film surface can thus be followed by continuous monitoring of the resonance angle. A detection volume is defined by the size of the illuminated area at the interface and the penetration depth of the evanescent field. It is noteworthy that no light passes through the detection volume. The optical device on one side of the metal film detects changes in the refractive index in the medium on the other side. Extensive theoretical treatments of the SPR phenomenon may be found in refs. 14 and 15.

Instrumentation

The instrument consists of a processing unit, reagents for ligand immobilization, exchangeable sensor chips and a personal computer for control and evaluation. The processing unit contains the SPR monitor and an integrated microfluidic cartridge that, together with an autosampler, controls the delivery of sample plugs into a transport buffer that passes continuously over the sensor chip surface (Fig. 1).

Fig. 2 shows the configuration of the SPR detector, the sensor chip and the microfluidic cartridge. The sensor chip is held in contact with the prism of the optical system by the microfluidic cartridge. Plane polarized light from a high-efficiency near-infrared LED is focused in a transverse wedge,

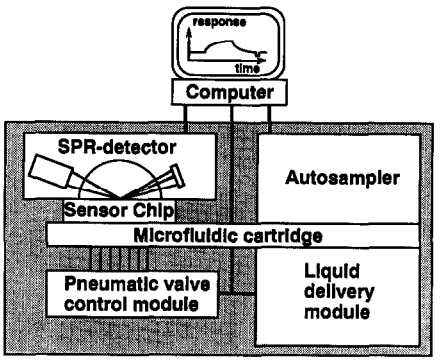

Fig. 1. The processing unit contains the SPR detector and an integrated microfluidic cartridge that, together with an autosampler, controls the delivery of sample plugs into a transport buffer that passes continuously over the sensor chip surface. Pneumatic valves in the microfluidic cartridge direct the flow.

through the prism on to the side of the sensor chip opposite to the gold layer. Reflected light is monitored by a fixed two-dimensional array of light-sensitive diodes, placed so that the resolution between diodes correspond to a difference in reflected angle of 0.1°. Computer interpolation routines process the data from the diode array to determine the position of the resonance angle to an accuracy of 10^{-4}°. Averaged readings are obtained at a frequency of 5 Hz. The use of a fixed detector array eliminates moving parts from the optical system,

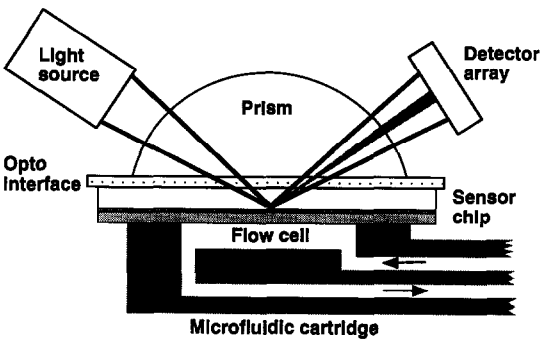

Fig. 2. The SPR detector, sensor chip and flow cell are shown docked together. Light from the LED is coupled to the sensor chip via a prism. The position of the reflectance minimum is monitored continuously by a photodiode array. When a molecule introduced via the flow cell is captured at the sensor surface, the position of the reflectance minimum will change. In the instrument, a wedge-shaped light beam and a two-dimensional detector array permit monitoring of four flow channels formed by docking the microfluidic cartridge against the sensor chip.

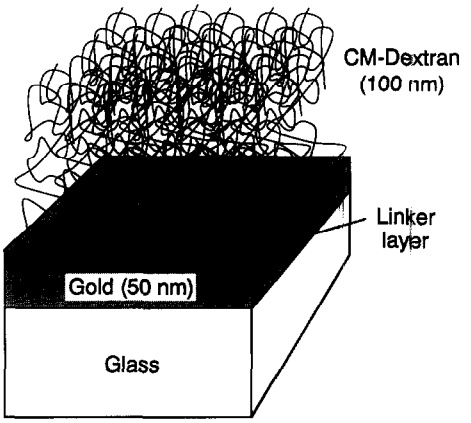

Fig. 3. The sensor chip consists of a 50-nm gold film deposited on a glass slide. A linker layer totally covers the gold film and acts as an anchor for the dextran matrix, which extends about 100 nm into solution.

increasing the reliability of the instrument and allowing changes in resonance angle to be followed in real time. A layer of silicone polymer, matched in refractive index to the glass of the sensor chip, ensures exact optical contact between the removable sensor chip and the fixed parts of the optical system.

The microfluidic cartridge [16] contains two identical sets of pneumatic valves and channels, each with two sample loops for injection of volumes up to 5 and 45 μl, respectively. At the surface of the cartridge a flow cell block with four channels is located. When the cartridge is docked against the sensor chip, four parallel flow cells, each with a volume of 60 nl, are formed. The four flow cells, which are illuminated simultaneously by the transverse wedge of light, can be connected to any of the sample loops through the valves.

The sensor chip (Fig. 3) consists of a glass substrate on to which a 50-nm thick gold film has been deposited. The gold film is then covered with a long-chain hydroxyalkanethiol which forms a monolayer at the surface. This layer serves both as a barrier to prevent proteins and other ligands from coming into contact with the metal and as a functionalized structure to which a matrix of dextran is attached. The dextran, which extends typically 100 nm out from the surface, makes it possible to exploit the penetration depth of the evanescent field creating a volume in which molecular interactions can be studied [17]. By using a carboxymethylated dextran, substances containing primary amine functions can be immobilized after activation of the matrix with carbodiimide–N-hydroxysuccinimide [18].

Sensor chip chemistry

The first experimental step is to immobilize a ligand to the sensor surface. The ligand may be one of the reactants in the interaction of interest or, *e.g.*, an antibody that can capture one of the reactants. The immobilization, which is performed with the sensor chip *in situ* in the instrument, is continuously monitored by the SPR detector (Fig. 4). This allows direct comparison of the amount immobilized between all surfaces prepared. The method utilizes the formation of N-hydroxysuccinimide esters from a fraction of the carboxyl groups of the carboxymethyldextran matrix via reaction with N-hydroxysuccinimide and N-ethyl-N'-(dimethylaminopropyl)-carbodiimide hydrochloride in water. In a second step, the protein is passed over the surface in a solution of low ionic strength with a pH value below the isoelectric point of the protein. The protein is thereby concentrated in the matrix by electrostatic attraction forces and a simultaneous reaction with the active esters takes place. In a final step, the remaining active esters are converted into amides via reaction with ethanolamine. The immobilization, which requires typically less than 30 min, can be controlled by parameters such as protein concentra-

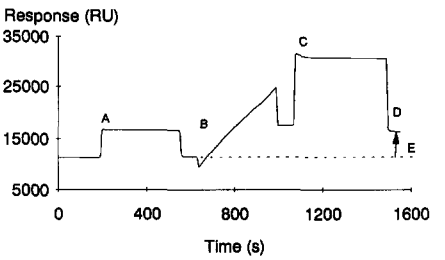

Fig. 4. As the SPR detector senses all changes in the RI close to the surface, all steps during immobilization can be followed. Initially the continuous buffer flows past the surface, and a reference baseline is registered. At A a pulse of EDC–NHS is injected to activate the matrix. After the pulse with a high RI has passed, the signal drops to the level corresponding to the continuous buffer. The RAMFc is then injected (B) and the progress of enrichment of antibodies in the matrix can be followed. Ethanolamine is then injected (C) to remove any remaining active esters and after conditioning with the regeneration solution to be used (D), the RAMFc surface is now ready for use. The amount immobilized is indicated at E.

tion, protein solution ionic strength and pH, reagent concentration and reaction times [17]. From reproducibility studies in which three different proteins were immobilized to 150 sensor chips from more than 10 batches, a precision of better than 4% (relative standard deviation) was obtained. These values include errors in the reagent preparation and in the precision of the production of sensor chips and the instrumental performance [17]. Depending on the stability of the immobilized ligand, the sensor surface can be regenerated and used for a series of analyses.

The sensorgram

By continuously monitoring the refractive index (RI) in the detected volume and plotting this value against time, a sensorgram is obtained. The ordinate of the sensorgram is denoted the resonance signal and is indicated in resonance units (RU); 1000 RU correspond to a 0.1° shift in the surface plasmon resonance angle and for the average protein this corresponds to a surface concentration change of about 1 ng mm^{-2} [19]. The total range covered by the SPR detector is 3°, corresponding to 30 000 RU. The resonance signal at a certain point in time will be the sum of the contributions from the sensor surface, the interacting molecules and the bulk solution. Under conditions of constant bulk RI, the amount of interacting molecules can be monitored continuously. Otherwise, the amount may be quantified by readings taken between sample injections, where the transport buffer of constant RI passes the sensor surface.

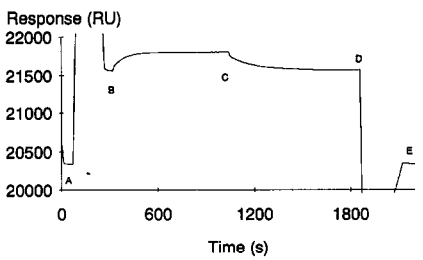

Fig. 5. The RAMFc surface prepared as described in Fig. 4 is used here to capture a MAb from a crude hybridoma culture supernatant (A). When the sample pulse has passed, the corresponding antigen is injected (B) and its association to the antibody can be followed. Gradually the interaction approaches a steady state and when the antigen solution is replaced by the continuous buffer (C), dissociation of the Ab–Ag complex can be seen. After removal of the MAb by a regenerating solution (D), the RAMFc surface is ready for the next analysis cycle (E).

Let us consider the sensorgram shown in Fig. 5. The sensor surface used has been prepared by immobilizing a polyclonal rabbit anti-mouse Fc (RAMFc) antibody as shown in Fig. 4. At the beginning of the run a continuous flow of buffer is passing the surface (A), resulting in a resonance signal of 20 350 RU. During the time span from A to B, a crude cell culture supernatant, containing a mouse monoclonal antibody (MAb), is introduced by switching one of the sample loops into the buffer flow. The instantaneous rise in the resonance signal as the sample enters the flow cell is due to the high RI of the culture supernatant. At B the sample plug has passed and buffer once again passes the surface. Here a resonance signal level of 21 550 RU can be read under the same conditions as in A. The signal shift from binding of the MAb to the RAMFc surface is thus 1200 RU. During time B to C, the antigen, corresponding to the captured MAb, is introduced. The signal gradually increases a further 250 RU. When buffer replaces the antigen solution (C), the dissociation of the MAb–antigen complex can be seen. By introducing a regenerating agent (D), the MAb is washed out and the signal drops back to its original level. The RAMFc surface is now ready for another analysis cycle (E).

This illustrates several features of the technique: (1) the selectivity of the sensor surface can be controlled by the operator through the immobilized molecule; (2) concentration determinations in crude samples can be made if a calibration graph is constructed; (3) different unlabelled molecules can be injected in series and each interaction quantified, allowing stoichiometric calculation on the complex formed; (4) the progress of association and dissociation events can be followed, providing a basis for kinetic studies; and (5) once the regeneration conditions have been optimized, usually 50–100 cycles can be run without loss of activity.

RESULTS AND DISCUSSION

Kinetic analysis

For a one to one interaction in solution between reactants A and B which can form a complex AB, the rate of formation of AB complexes at time t may be written as

$$d[AB]/dt = k_{ass}\,[A]_t\,[B]_t - k_{diss}\,[AB]_t$$

where k_{ass} is the association rate constant (l mol^{-1} s^{-1}) and k_{diss} is the dissociation rate constant (s^{-1}), and after substituting $[B]_t$ for $[B]_0 - [AB]_t$, where $[B]_0$ is the total concentration of reactant B, as

$$d[AB]/dt = k_{ass}\,[A]_t\,([B]_0 - [AB]_t) - k_{diss}\,[AB]_t$$

In the biosensor, one of the reactants is immobilized to the sensor surface and the other is continuously replenished from a solution flowing past the sensor surface. The response R will correspond to the amount of AB complexes formed and the maximum response R_{max} will be proportional to the surface concentration of the immobilized ligand. The rate equation can thus be rewritten as

$$dR/dt = k_{ass}\,C\,(R_{max} - R_t) - k_{diss}\,R_t$$

where dR/dt is the rate of formation of surface complexes, *i.e.*, the derivative of the observed response curve, C, which is kept constant, is the concentration of analyte in free solution, R_{max} is the total amount of binding sites of the immobilized ligand expressed as SPR response and $R_{max} - R_t$ is the amount of remaining free binding sites at time t. Note that as terms in R occur on both sides of the equation, the response value R_t can be used directly without conversion between response and absolute concentration of complexes formed on the sensor chip surface.

Rearranging the rate equation shows more clearly that the derivative of the binding curve is linearly related to the response. In principle, therefore, k_{ass} and k_{diss} can be calculated from the straight line obtained by plotting of dR/dt *versus* R:

$$dR/dt = k_{ass}\,C\,R_{max} - (k_{ass}\,C + k_{diss})\,R_t$$

This, however, requires a knowledge of the saturation response R_{max}, which can be assessed from an injection of the free analyte at very high concentration. This approach is therefore often unrealistic, especially if precious samples are to be handled.

If, however, dR/dt *versus* R plots are made for a range of concentrations, C, of the free analyte, each of the lines will have a slope, k_s, corresponding to $k_{ass}\,C + k_{diss}$. If then the k_s values are plotted *versus* concentration, the new line obtained will have a slope corresponding to k_{ass} and an intercept with the k_s axis corresponding to k_{diss}.

When the sample pulse has passed the surface, the concentration C of free analyte suddenly drops to zero and dissociation will then be observed according to

$$dR/dt = -k_{diss}\,R_t \quad \text{or} \quad \ln(R_0/R_n) = k_{diss}\,(t_n - t_0)$$

where R_n is the response at time n and R_0 is the response at an arbitrary starting time zero. The dissociation rate constant k_{diss} is thus obtained as the slope of the $\ln(R_0/R_n)$ *versus* $(t_n - t_0)$ plot.

Kinetic analysis of monoclonal antibody–antigen interactions using the system described here has recently been published [20,21] and also a discussion on other applications and the range of rate constants measured [22]. As an example of kinetic analysis we report here a study of the interaction between insulin-like growth factor I (IGF-I) and IGF binding protein 1 (IGFBP-1). A surface prepared by immobilizing IGFBP-1 is used to obtain binding curves for IGF-I in the concentration range 10.2–163.4 nM (Fig. 6). A plot of the derivative dR/dt *versus* relative response R, *i.e.*, the response relative to the baseline prior to the injection, covering the whole injection for one of the concentrations used is shown in Fig. 7. The plot is not the expected straight line for the following reasons. Initially (phase A in Fig. 7), during the transition from continuous buffer to sample and due to sample dispersion, some time will elapse before the sample has replaced the continuous buffer in the flow cell. A constant concentration has

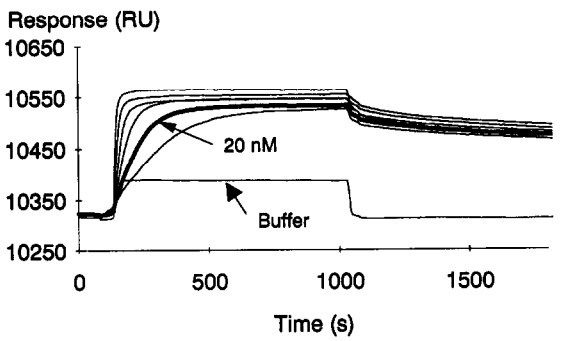

Fig. 6. Overlay plot of sensorgrams of the interaction of IGF-I in solution with IGFBP-1 immobilized to the sensor chip; 15-min injections of IGF-I at concentrations of (from bottom to top) 10, 20, 40, 80 and 160 nM were done at a flow-rate of 2 μl min^{-1} followed by dissociation in buffer flow for 15 min. Shown also is the shape of a salt pulse to illustrate the parts of the sensorgram where sample zone dispersion occurs.

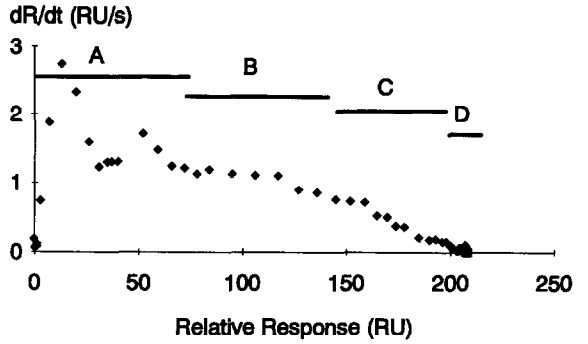

Fig. 7. Plot of the derivative (dR/dt) *versus* relative response (R) for 20 n*M* IGF-I, *i.e.*, the bold curve in Fig. 6. During the first 30 s (A) the data mainly reflect sample dispersion and a change in bulk RI. During phase B, mass transport is the rate-limiting factor. When the response has reached about 140 RU the remaining binding site concentration is low enough to reflect the interaction. At D a steady state is reached and hence the binding rate is zero.

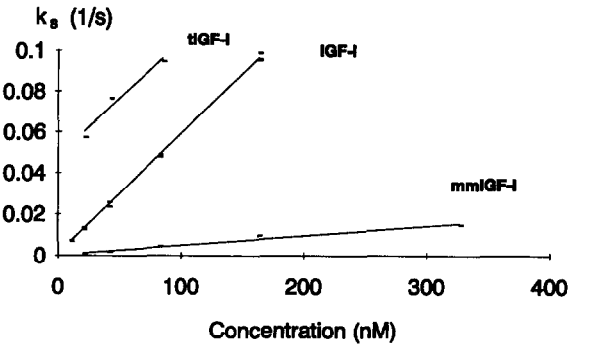

Fig. 9. Plots of the concentration dependence of slopes (k_s) of the binding curves for native, truncated and mismatched IGF-I. The slopes of the plots correspond to the association rate constant k_{ass} and the intercept with the ordinate to the dissociation rate constant k_{diss}. The parallelism of the plots for the native and truncated forms indicate similar k_{ass} values whereas the intercepts indicate similar and low k_{diss} value for native and mismatched IGF-I.

to be reached, not only for the sample molecules, but also for the bulk buffer solution. The apparently high initial binding rate can in fact mainly be attributed to a rapid increase in the bulk RI. During phase B, even though surface binding sites are consumed, as reflected by the continuously increasing response, the expected drop in binding rate does not occur. Here the rate of binding is limited by the rate at which mass transport by diffusion occurs from the bulk sample solution into the dextran matrix. Under conditions where mass transport is the limiting factor, the observed binding rate is dependent on the bulk solution flow-rate [23] since a change in flow-rate will change the thickness of the unstirred layer close to the sensor chip surface across which diffusion takes place. As binding proceeds a situation will eventually be reached (phase C) where the binding rate is dominated by the interaction *per se*, and hence in this region relevant binding data can be collected. Finally (phase D), equilibrium between the association and dissociation rates for this particular concentration is reached. Fig. 8 summarizes the reaction rate limited data obtained for all five concentrations used.

The dependence of the slope of the binding curve on the concentration of native IGF-I and of two structural variants, tIGF-I and mmIGF-I, is shown

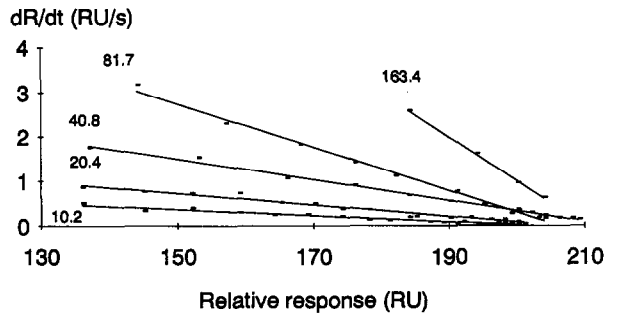

Fig. 8. Plots of dR/dt *versus* R data obtained during the reaction rate-limited phase for the five concentrations used. The slopes (k_s) of these plots are transfered to Fig. 9.

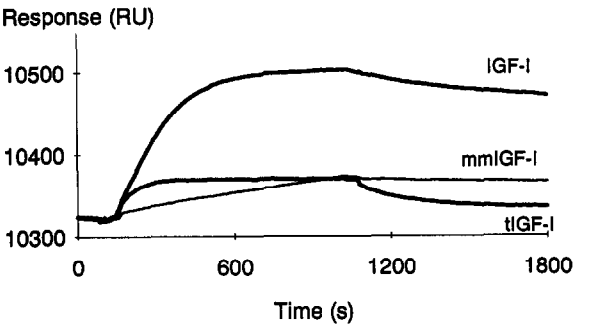

Fig. 10. Sensorgrams for the three forms of IGF-I all recorded at a concentration of 10 n*M*. From the levels of the steady-state responses, which during the injection are reached for the native and truncated forms, the native form showing a higher level can be judged to have a higher affinity. Obvious also is the comparatively high dissociation rate of the truncated form.

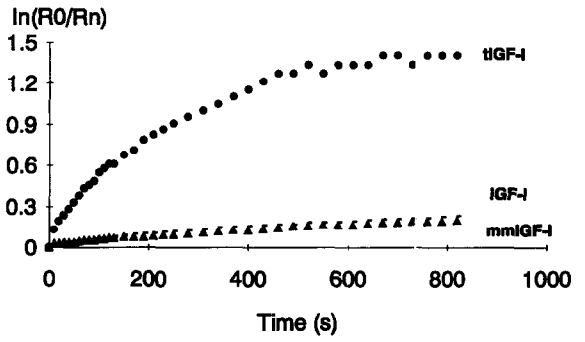

Fig. 11. Dissociation plots obtained from the progress of the sensorgrams during 15 min starting from where buffer has replaced the samples. During this time interval only the truncated form dissociates completely. A comparison with Fig. 9 shows the same distribution of the dissociation rate constants, *i.e.*, a high value for the truncated form and significantly lower and similar values for the native and mismatched forms.

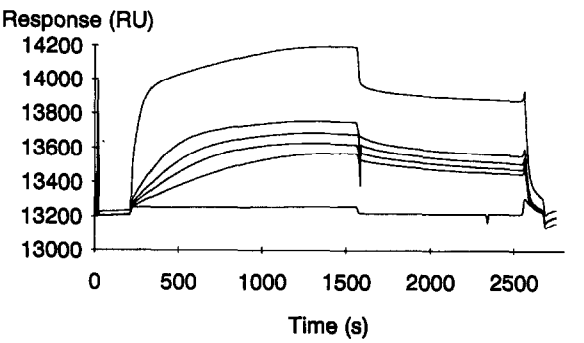

Fig. 12. Sensorgrams for the interaction between matrix-bound *lac* operator DNA (110 RU) and a fusion protein between the *lac* repressor and β-galactosidase. The repressor was injected for 22 min at a flow-rate of 2 μl min^{-1} and concentrations were, from bottom to top, 0.4, 0.6, 0.8, 1.2 and 5.0 μg ml^{-1}. Dissociation in buffer flow was monitored for 15 min. The biotinylated *lac* operator DNA was immobilized to the surface via covalently bound streptavidin. Removal of the *lac* repressor between runs were done by injection of a 0.05% sodium dodecyl sulphate solution. No attempts were made to regenerate the surface down to the streptavidin level.

in Fig. 9. tIGF-I is a truncated form, lacking three amino acid residues at the N-terminus, and mmIGF-I contains erroneous disulphide pairing. From the parallelism of the plots for the native and truncated forms, the association rate constants k_{ass} are obviously similar, and were calculated to be $5.8 \cdot 10^5$ and $5.7 \cdot 10^5$ l mol^{-1} s^{-1}, respectively. For the form containing disulphide mismatches, k_{ass} was found to be decreased to $4.6 \cdot 10^4$ l mol^{-1} s^{-1}. The k_{diss} values as reflected in the plot (the intercept with the ordinate), on the other hand, indicate low and similar values for the native and mismatched forms. However, as the data were collected during the association phase of the sensorgram, the dominance of the association rate constant on the progress of the binding introduces a substantial uncertainty in the values when determined from the intercepts. A direct comparison of the sensorgrams recorded using identical concentrations of the three IGF-I variants as shown in Fig. 10 provides a simple means of qualitative comparison of their kinetic and affinity properties. From the levels of the steady-state responses, which during the injection are reached for the native and truncated forms, the native form showing a higher level can be judged to have higher affinity. Obvious also is the comparatively high dissociation rate of the truncated form. Disscociation plots obtained from the progress of the sensorgrams during 15 min starting from where buffer has replaced the samples is shown in Fig. 11. The reason for the decreasing slope of the plots and hence decreasing k_{diss} with time is not obvious. It might reflect heterogeneity in one or both of the interactants or, taking into account that the residence time for the sample molecules varies from 0 to 15 min, a time-dependent "maturation" of the interaction itself on the molecular level. However, independent of at what time slope values are selected for rate constant calculations, the ranking between the three IGF forms is the same. Using the initial slope, k_{diss} was calculated to be $1.3 \cdot 10^{-3}$ s^{-1} for the native form, $1.2 \cdot 10^{-3}$ s^{-1} for the mismatched form and $7.7 \cdot 10^{-3}$ s^{-1} for the truncated form. A comparison of the information in Figs. 9 and 11 gives the same

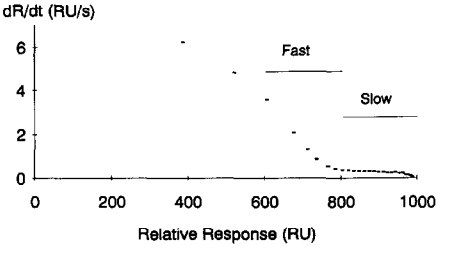

Fig. 13. Plot of the derivative (dR/dt) *versus* relative response (R) for the *lac* operator DNA–*lac* repressor interaction at a repressor concentration of 5 μg ml^{-1}, *i.e.*, the highest concentration shown in Fig. 12. Once the initial mass transport limited phase has passed, the reaction progresses through two stages. After a high initial binding rate a second stage of much slower binding is seen.

distribution of the dissociation rate constant, with a high value for the truncated form and significantly lower and similar values for the native and mismatched forms.

As a second example of kinetic analysis, the interaction between matrix bound *lac* operator DNA and a fusion protein between the *lac* repressor and β-galactosidase is shown. The *lac* operator DNA, a synthetic 35-base pair DNA with one strand biotinylated at the 5′-end, was captured by streptavidin immobilized at the sensor chip. A series of injections of repressor protein covering the concentration range 0.4–5 $\mu g\ ml^{-1}$ (0.7–8.3 n*M*) was done as shown in Fig. 12. From the shape of the binding curves, which is more clearly seen at higher repressor concentrations, the interaction appears to be hetero-

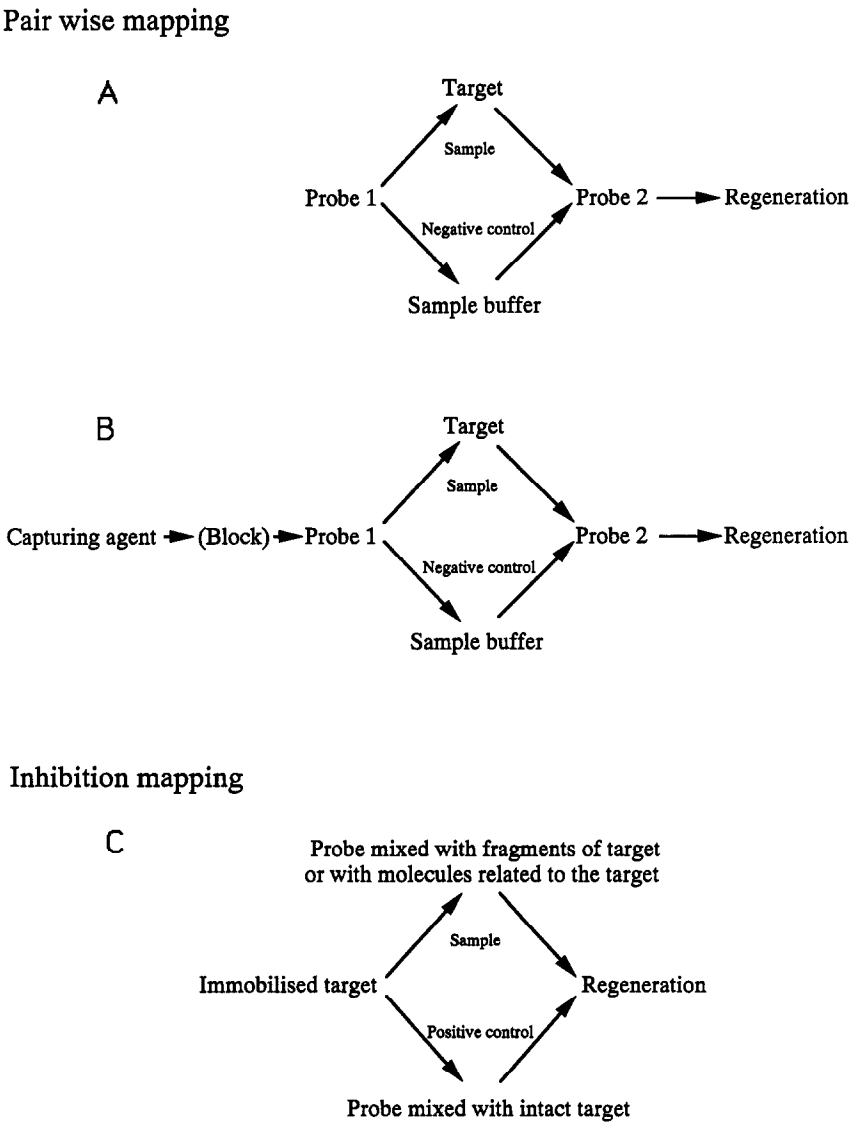

Fig. 14. Summary of the three approaches to binding site analysis. Pairwise mapping is either performed with the primary probe immobilized directly to the surface (A) or indirectly by a capturing agent (B). In inhibition mapping, the target molecule is immobilized to the surface and probes mixed with potential inhibitors are injected.

geneous. After a high initial binding rate the curve reaches a second stage of much slower binding. A plot of the binding rate (dR/dt) *versus* relative response (R) as in Fig. 13 shows this more clearly. The average association rate constant for the specific (fast) interaction calculated from three separate experiments using varying amounts of immobilized DNA was $4.0 \cdot 10^6$ l mol^{-1} s^{-1}, with a range from $2.1 \cdot 10^6$ to $5.8 \cdot 10^6$ l mol^{-1} s^{-1}. From the same set of experiments the non-specific (slower) interaction was calculated to have an average association rate constant of $9.0 \cdot 10^4$ l mol^{-1} s^{-1}. Measurements in the presence of the inhibitor isopropyl thiogalactoside resulted in a calculated association rate constant of $3.1 \cdot 10^4$ l mol$^{1-1}$ s^{-1}. In control experiments (not shown) using non-specific polyoma virus DNA, the association rate constant was calculated to be $3.1 \cdot 10^4$ l mol^{-1} s^{-1}. The dissociation rate constant, determined in three separate experiments using operator DNA, was calculated to be $3.2 \cdot 10^{-4}$ s^{-1} (range $2.0 \cdot 10^{-4}$–$4.7 \cdot 10^{-4}$ s^{-1}) and differed little from that obtained using non-specific polyoma virus DNA. Affinity constants, calculated as the ratio between association and dissociation rate constants, were $1.5 \cdot 10^{10}$ and $5.8 \cdot 10^7$ l mol^{-1} for the specific and the non-specific interactions, respectively. From experiments performed by a membrane filtering technique using native *lac* repressor protein and *lac* operator carried on $\lambda\varphi 80$ d*lac* phage DNA, the reported affinity constant in free solution is 10^{13} l mol^{-1} in 10 m*M* KCl and $4.2 \cdot 10^{11}$ l mol^{-1} in 150 m*M* KCl [24]. The lower values obtained in our determinations may in part be attributed to the differences in the experimental procedures but probably more to the effect on the association rate constant caused by the use of a fusion protein (MW $600 \cdot 10^3$) rather than the native repressor (MW $148 \cdot 10^3$). In a study using the native repressor protein, the non-specific interaction described here was not as pronounced [25], indicating that it may be an artefact induced by the fusion protein.

Binding site analysis

Binding site analysis, or the elucidation of the pattern by which a set of molecules interact, is a powerful tool for obtaining information on the topology of a target molecule and for identifying structural motifs of importance for its function. Epitope mapping using monoclonal antibodies as molecular probes is well established, and a methodology using SPR detection has been described previously [26]. As an example of binding site analysis, we describe here the results obtained for a set of molecules consisting of insulin-like growth factors I and II, insulin-like growth factor binding protein-1 (IGFBP-1), four IGFBP-1 specific monoclonal antibodies and two IGFBP-1 derived peptides, where IGFBP-1 is the target molecule.

The three approaches to binding site analysis used here are summarized in Fig. 14 and can be classified as either pairwise mapping, where the target molecule is probed by a pair of molecules with the

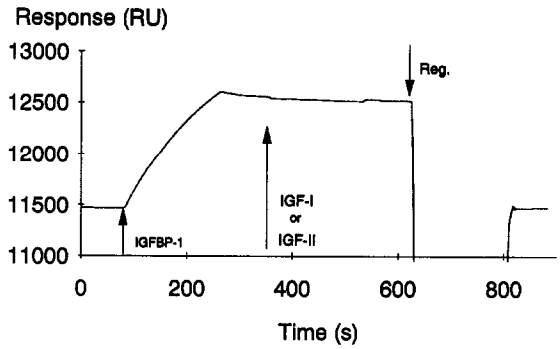

Fig. 15. Pairwise mapping. Overlay of two sensorgrams where IGFBP-1 was first injected (6 μl, 50 μg ml^{-1}) over an IGF-I surface followed by either IGF-I or IGF-II (4 μl, 20 μg ml^{-1}) at a flow-rate of 2 μl min^{-1}. The absence of a response for the IGFs indicates that there is only a single binding site on IGFBP-1 for IGF, and that even though they might not be identical for the two types, the binding of one form excludes the binding of the other.

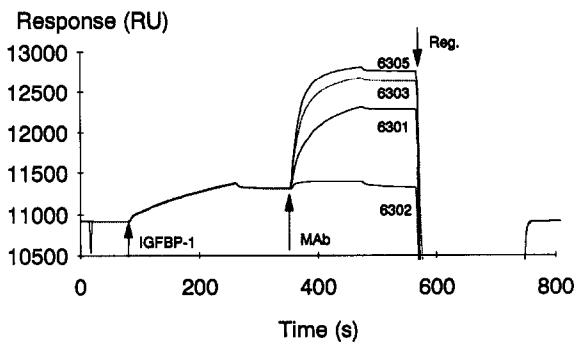

Fig. 16. Pairwise mapping. Overlay of four sensorgrams where IGFBP-1 was first injected (6 μl, 50 μg ml^{-1}) over an IGF-I surface followed by one of four MAbs (4 μl, 10–100 μg ml^{-1}) at a flow-rate of 2 μl min^{-1}. Only MAb 6302 is excluded from binding by the IGFBP-1–IGF-I interaction.

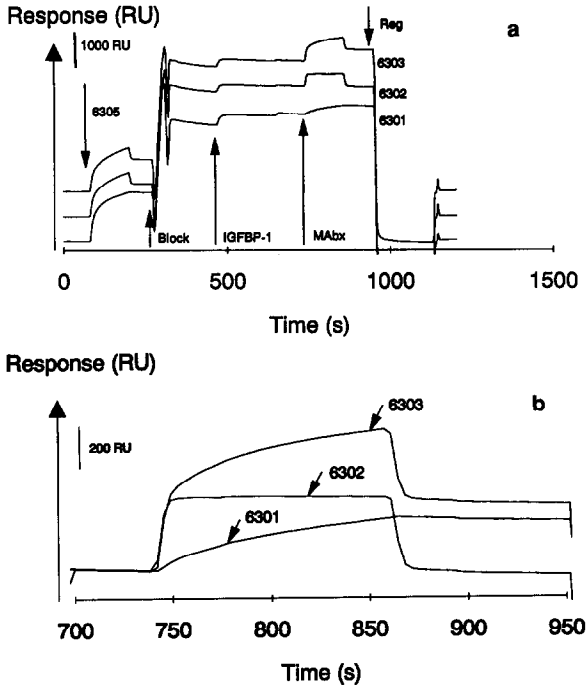

Fig. 17. (a) Pairwise mapping. Overlay of three complete sensorgrams where MAb 6305 (4 μl, 100 μg ml^{-1}) was first captured by surface-immobilized RAMFc. To block remaining MAb reactive surface sites, a non-specific MAb was then injected (4 μl). The target molecule IGFBP-1 was then injected (6 μl, 50 μg ml^{-1}) followed by the second MAb (4 μl, 10–100 μg ml^{-1}). (b) Binding curves for the three secondary MAbs, enlarged. No increase in the response was observed for MAb 6302, only a bulk RI shift during the injection.

primary probe immobilized at the surface and the other one introduced after the target molecule, or as inhibition mapping, where the target molecule is immobilized to the surface and is challenged with a probe preincubated with a fragment of the target molecule. When, in pairwise mapping, the surface-bound primary probe is a monoclonal antibody, the use of a general capturing agent such as RAMFc is economical as the same covalently immobilized surface can be used to capture different primary probes.

In a first experiment of pairwise mapping, the number of sites on IGFBP-1 for binding of IGF-I and IGF-II was investigated (Fig. 15). IGF-I was immobilized to the sensor surfac and after binding of IGFBP-1 a second injection of either IGF-I or IGF-II was done. The absence of a response indicates that there is only a single binding site on

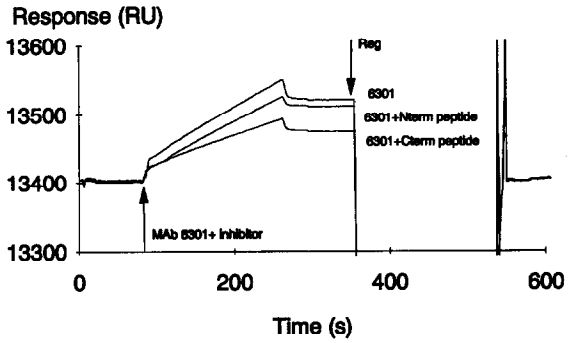

Fig. 18. Inhibition mapping. Surface-immobilized IGFBP-1 was probed with either MAb 6303 alone (15 μl, 1 μg ml^{-1}) or preincubated with peptides derived from the N- or C-terminus of IGFBP-1 (15 μl, 1 μg ml^{-1} MAb and 10 μg ml^{-1} peptide). A significant inhibitory effect is observed for the N-terminal peptide.

IGFBP-1 for IGF, and that even though they might not be identical for the two types, the binding of one form excludes the binding of the other. Also, using an IGF-I surface, the possibility of concurrent binding to IGFBP-1 of IGF-I and each of the four MAbs was tested (Fig. 16). Only one of the MAbs (6302) was excluded from binding by the IGFBP-1–IGF-I interaction. The difference in the response levels between the three reacting MAbs can be ascribed to differences in both concentration and kinetic properties.

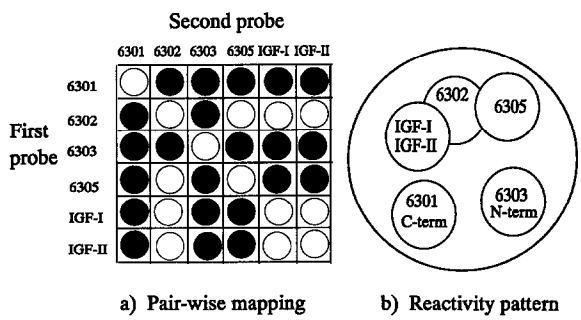

Fig. 19. (a) Reactivity pattern matrix. Rows indicate primary probes and columns secondary probes. Filled circles denote pairs of probes that can bind concurrently. From the matrix it can be seen that two of the MAbs (6301 and 6303) only interfere with themselves and that IGF-I and IGF-II show the same pattern. The most complicated pattern was obtained for MAb 6302, which interferes both with MAb 6305 and with the two growth factors. (b) Transformation of the data in (a) to a "surface like" map. Overlapping circles denote pairs of probes that mutually interfere in binding to IGFBP-1.

Next, IGFBP-1 was probed with pairs of MAbs (Fig. 17). Here a rabbit anti-mouse Fc (RAMFc) surface was used to capture the first MAbs. The same covalently immobilized surface could therefore be used to test any combination of the MAbs in any order. To suppress a false response from interaction between the second MAb and the RAMFc surface, any binding sites remaining after introduction of the first MAb are blocked by injection of a saturating concentration of a non-specific MAb of the same subclass as the second MAb [26]. Using MAb 6305 as the primary probe excluded only MAbs 6302 from binding. Analogous experiments substituting the second antibody with IGF-I or IGF-II revealed that only MAb 6302 blocked the growth factor binding site on IGFBP-1.

An example of inhibition mapping using an IGFBP-1 surface which is probed by one of the MAbs is shown in Fig. 18. Here the inhibitory effect of two peptides, derived from the N and C termini of IGFBP-1, on the binding of a MAb was tested. After preincubation of the MAb with peptides or buffer as control, the binding rates were compared. A pronounced inhibitory effect was found in this case for the N-terminal peptide, indicating that the epitope defined by MAb 6303 is located in this part of the IGFBP-1 molecule.

The results of the total pairwise binding site analysis are compiled in Fig. 19a as a reactivity pattern matrix. The "checker board" representation was constructed by indicating whether pairs of probes could bind concurrently or not. Rows indicate primary probes and columns secondary probes. Note that the matrix is symmetrical, *i.e.*, in none of the cases did the inversion of the order of binding change the result. From the matrix it can be seen that two of the MAbs (6301 and 6303) only interfere with themselves and that IGF-I and IGF-II show the same pattern. The most complicated pattern was obtained for MAb 6302, which interferes both with MAb 6305 and with the two growth factors. A visually more easily interpretable representation of the data is shown in Fig. 19b.

Concentration analysis

Fundamental descriptors of any analytical technique are performance characteristics such as reproducibility, repeatability, sensitivity and, for concentration analysis, the working range as specified by the accepted relative standard deviation [27]. To illuminate some of these characteristics of the technology presented here, concentration analysis of an analyte β_2-microglobulin ($\beta_2\mu$), used as a reference

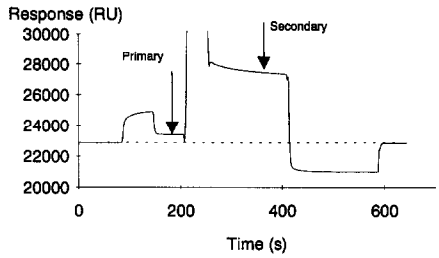

Fig. 20. Sensorgram describing the assay cycle used for concentration determination of β_2-microglobulin. The biospecific surface consists of a covalently immobilized anti-β_2-microglobulin monoclonal antibody. Points where primary and secondary response values are collected relative to the initial baseline are indicated as 1′ and 2′.

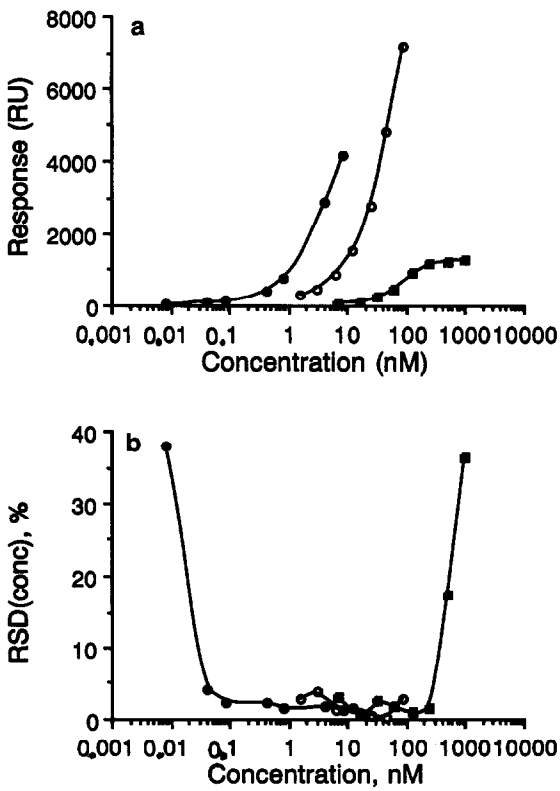

Fig. 21. (a) Calibration graphs for the three intervals. (b) Precision profiles for the three concentration ranges. ● = Secondary; 7 min; ○ = secondary, 1 min; ■ = primary.

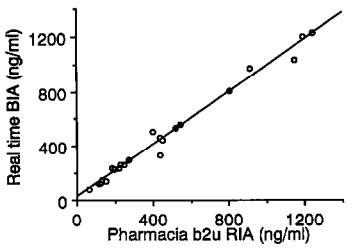

Fig. 22. Correlation curve for β_2-microglobulin in human serum for the intermediate concentration range (19–1058 ng ml^{-1}) between the secondary response for 1-min injections and a radioimmunoassay, Pharmacia $\beta_2\mu$ RIA.

during system development, is briefly described. Details on the "fine tuning" of concentration analysis in terms of surface ligand density, regeneration conditions, selection of primary and secondary reagents, etc., will be published elsewhere [28]. Using SPR detection, the response can be measured either directly as that of the analyte exposed to the biospecific surface or, secondarily, as the response from a subsequently introduced analyte-specific reagent. The secondary reagent, apart from enhancing the signal, also acts as a means of increasing the specificity of the signal when low analyte levels are measured in crude samples that can cause a non-specific or background noise signal.

The assay procedure described utilizes a $\beta_2\mu$ specific monoclonal antibody as the capturing agent. Under the conditions used (a high surface density and a high association rate of the capturing antibody), mass transport of the analyte to the sensor surface rather than the reaction between antibody and analyte will be the binding rate limiting factor. The primary response is therefore proportional to the contact time between the sample and sensor surface and to the concentration of the analyte. This means that the position of the calibration graph, keeping everything else constant, can be adjusted over a wide concentration range simply by adjusting the sample injection time. When a secondary reagent is used, rapid saturation of the analyte is wanted and it is therefore injected at a high concentration. A sensorgram describing the analysis cycle is shown in Fig. 20.

Calibration graphs covering the concentration range from 8.3 pM to 1 μM (0.1 ng ml^{-1} to 12 μg ml^{-1}) of $\beta_2\mu$, *i.e.*, a 10^5-fold span, together with the corresponding precision profiles for five replicates of each determination are shown in Fig. 21. As can be seen, relative standard deviation of better than 5% was obtained for the interval from 40 pM to 250 nM. Note that for each calibration graph all determinations were done using the same sensor chip and hence include regeneration of the surface and, for the two lower ranges, also injection of a secondary reagent.

The intermediate concentration range covered by a 1-min injection in combination with a secondary reagent enhancement was compared with a commercially available radioimmunoassay, Pharmacia $\beta_2\mu$ RIA, in a correlation study (Fig. 22). Twenty-four human serum samples covering the concentration range 19–1040 ng ml^{-1} were tested in duplicate by both methods. The regression line obtained, calculated by the least-squares method, was $y = 0.9653x - 13.8$ (ng ml^{-1}), where x is the Pharmacia RIA and y is the biosensor method. The correlation coefficient (r) was 0.99, indicating excellent agreement.

We define the sensitivity of the assay as the concentration at which a response three standard deviations above that for a zero dose is obtained. For a 7-min injection using a secondary reagent, it was calculated to be 25 pM.

ACKNOWLEDGEMENTS

The authors thank Dr. Maris Hartmanis, Kabigen, where R. Karlsson performed the IGBP-1-related work during an 8-week stay, Dr. Lars Holmberg, Kabi Pharmacia, for synthesizing the biotinylated *lac* operator DNA, and Dr. Mats Nilsson, Institute of Medical Virology, Biomedical Centre, University of Uppsala, for supplying the biotinylated polyoma virus DNA.

REFERENCES

1 L. Vroman and A. L. Adams, *Surf. Sci.*, 16 (1969) 438–446.
2 R. M. Sutherland, C. Dähne, J. F. Place and A. R. Ringrose, *Clin. Chem.*, 30 (1984) 1533–1538.
3 B. Liedberg, C. Nylander and I. Lundström, *Sensors Actuators*, 4 (1983) 299–304.
4 E. Kretschmann and H. Raether, *Z. Naturforsch.*, 23 (1968) 2135–2136.
5 A. Otto, *Z. Phys.*, 216 (1968) 398–410.
6 H. Raether, in G. Hass, M. Francombe and R. Hoffman (Editors), *Physics of Thin Films*, Vol. 9, Academic Press, New York, 1977, pp. 145–261.

7 D. C. Cullen, R. G. W. Brown and C. R. Lowe, *Biosensors*, 3 (1987/1988) 211–225.
8 M. T. Flanagan and R. H. Pantell, *Electron. Lett.*, 20 (1984) 968–970.
9 P. B. Daniels, J. K. Deacon, M. J. Eddowes and D. G. Pedley, *Sensors Actuators*, 15 (1988) 11–18.
10 R. P. H. Kooyman, H. Kolkman, J. van Gent and J. Greve, *Anal. Chim. Acta*, 213 (1988) 35–45.
11 C. S. Mayo and R. B. Hallock, *J. Immunol. Methods*, 120 (1989) 105–114.
12 D. C. Cullen and C. R. Lowe, *Sensors Actuators*, B1 (1990) 576–579.
13 M. N. Kronick and W. A. Little, *J. Immunol. Methods*, 8 (1975) 235–240.
14 A. D. Boardman (Editor), *Electromagnetic Surface Modes*, Wiley, Chichester, 1982.
15 H. Raether, *Surface Plasmons on Smooth and Rough Surfaces and on Gratings*, Springer, Berlin, 1988.
16 S. Sjölander and C. Urbaniczky, *Anal. Chem.*, 63 (1991) 2338–2345.
17 S. Löfås and B. Johnsson, *J. Chem. Soc., Chem. Commun.*, (1990) 1526–1528.
18 B. Johnsson, S. Löfås and G. Lindquist, *Anal. Biochem.*, 198 (1991) 268–277.
19 E. Stenberg, B. Persson, H. Roos and C. Urbaniczky, *J. Colloid Interface Sci.*, 143 (1991) 513–526.
20 R. Karlsson, A. Michaelsson and L. Mattsson, *J. Immunol. Methods*, (1991) in press.
21 R. Karlsson, D. Altschu and M. H. V. van Regenmortel, in M. H. V. van Regenmortel (Editor), *Structure of Antigens*, Vol. 1, CRC Press, Boca Raton, FL, 1991, in press.
22 I. Chaiken, S. Rose and R. Karlsson, *Anal. Biochem.*, in press.
23 J. D. Andrade, in J. D. Andrade (Editor), *Surface and Interfacial Aspects of Biomedical Polymers* (*Surface Chemistry and Physics*, Vol. 2), Plenum Press, New York, 1986, p. 1.
24 A. D. Riggs, H. Suzuki and S. Bourgeois, *J. Mol. Biol.*, 48 (1970) 67–83.
25 K. Bondesson and Å. Frostell-Karlsson, in preparation.
26 L. G. Fägerstam, Å. Frostell, R. Karlsson, M. Kullman, A. Larsson, M. Malmqvist and H. Butt, *J. Mol. Recognition*, 3 (1990) 208–214.
27 R. Ekins, *Ligand Q.*, 4 (1981) 33–44.
28 I. Rönnberg, V. Johansson and K. Lagerström, in preparation.